Journal of Power Sources 190 (2009) 578–586

Contents lists available at ScienceDirect

Journal of Power Sources

journal homepage: www.elsevier.com/locate/jpowsour

Theoretical and experimental specific capacitance of polyaniline in sulfuric acid

Hanlu Li [a], Jixiao Wang [b,*], Qingxian Chu [b], Zhi Wang [b], Fengbao Zhang [a], Shichang Wang [b]

[a] Department of Chemical Engineering, School of Chemical Engineering and Technology, Tianjin University, Tianjin 300072, PR China
[b] State Key Laboratory of Chemical Engineering, Chemical Engineering Research Center, School of Chemical Engineering and Technology, Tianjin University, Tianjin 300072, PR China

ARTICLE INFO

Article history:
Received 13 June 2008
Received in revised form 13 December 2008
Accepted 19 January 2009
Available online 30 January 2009

Keywords:
Polyaniline
Nanofiber
Theoretical maximum specific capacitance
Diffusion
Heterogeneous

ABSTRACT

The theoretical mass specific capacitance (C_s) of polyaniline (PANI) is firstly estimated by combining electrical double-layer capacitance and pseudocapacitance. The maximum C_s is 2.0×10^3 F g^{-1} for one single PANI electrode. In present work, the PANI nanofiber modified stainless-steel (SS) electrode (PANI/SS) was used to assemble supercapacitors. Scanning electron microscopy (SEM) and transmission electron microscopy (TEM) images indicate that the PANI nanofiber has a coarse surface arising from the heterogeneous structure which likes an aggregation of nanoparticles. The performance of the assembled PANI/SS supercapacitors was investigated by cyclic voltammetry (CV), electrochemical impedance spectroscopy (EIS), and galvanostatic charge/discharge methods in 1.0 M H_2SO_4. The maximum C_s obtained from these methods in present work is 608, 445.0, and 524.9 F g^{-1}, respectively, which is only 30%, 22%, and 26% of the theoretical one. The significant difference between the experimental and the theoretical value indicates that only a low percentage of PANI (effective) has contribution to capacitance. The percentage of effective PANI depends on both the diffusion of dopants (counter-anions) and the conductivity of PANI. Under practical conditions, the former factor makes PANI nanofiber behave like a concentric cable with only the shell part involved in the charge/discharge process. The latter one which determines the electron transfer rate in PANI has an influence on the degree of redox reaction. In present work, the heterogeneous structure of the PANI nanofiber has a negative effect on the conductivity.

1. Introduction

Electrochemical supercapacitors have gained great interest in many advanced power systems requiring high power density, and high cycleability, such as in electric/hybrid vehicles, portable computers, cellular devices and nano-electronics [1–4]. The capacitance of supercapacitors can be divided into two basic types according to its charge storage mechanisms [5,6]: the one is electrical double-layer capacitance C_{dl}, which is generated from charge separation at electrode/electrolyte interface, and it is determined by the effective surface area and the dielectric constant of the electrolyte; and the other is pseudocapacitance C_p, which is generated from fast faradic reactions of the electrode material. Pseudocapacitance is produced from a bulk process whereas the double-layer capacitance is produced from a surface process.

Materials employed to assemble supercapacitor are mainly focused on carbon (including active carbon, carbon aero-gel, and carbon nanotube), metal oxides (including RuO_2, MnO_2, and IrO_2) and electrically conducting polymers (ECPs, including polyaniline, polypyrrole, and polythiophene). The charge storage of carbon is mainly produced from electrical double-layer capacitance mechanism, and the maximum available specific capacitance (C_s) of carbon has reached up to 320 F g^{-1} [7]. The charge storage of RuO_2 is mainly produced from the pseudocapacitance mechanism, and the available C_s of RuO_2 has reached up to 1170 F g^{-1} [8]. But RuO_2 is currently too expensive to be commercialized. ECPs have an advantage over noble metal oxides on their low cost, and have an advantage over carbon materials on large pseudocapacitance. The reversible faradic reactions of ECPs accompanied by doping/dedoping of dopants produce high pseudocapacitance. Due to these outstanding properties, ECPs have been intensively studied for supercapacitor application in recent years [9,10].

Polyaniline (PANI), one of the most studied ECPs, attracts considerable attention as a promising material in the application of supercapacitor because of inexpensive monomer and unique proton doping mechanism [11,12]. PANI has been investigated to modify various substrates (such as carbon [13,14], nickel [15], stainless-steel [16–20]) or blend with other materials (RuO_2 [21], carbon [22–26], and other ECPs [27]) for supercapacitor application. So far, the reported specific capacitance of pure PANI modified electrodes varies from 160 F g^{-1} to 815 F g^{-1} [13,15–20,22–26], and the highest value in 1.0 M H_2SO_4 is reported to reach 554 F g^{-1} wherein

* Corresponding author. Tel.: +86 22 27404533; fax: +86 22 27404496.
E-mail address: jxwang@tju.edu.cn (J. Wang).

0378-7753/$ – see front matter © 2009 Elsevier B.V. All rights reserved.
doi:10.1016/j.jpowsour.2009.01.052

the PANI was obtained by chemical oxidation [26] and reach to 742 F g^{-1} where the PANI was deposited by electrochemical polymerization [19]. What is the ultimate specific capacitance of PANI? What makes the specific capacitance so different? And what should we aim at?

Here, the maximum C_s of PANI (2.0×10^3 F g^{-1}) was estimated theoretically under the assumption that 100% of the PANI is oxidized or reduced in the charge/discharge process. The experimental results obtained by cyclic voltammetry (CV), electrochemical impedance spectroscopy (EIS), and galvanostatic charge/discharge methods are much lower than that of the theoretical one. The significant difference indicates that there is only a low percentage of PANI which has contribution to capacitance.

2. Experiment

2.1. Materials

Aniline was purified by distillation under reduced pressure and stored at 4 °C prior to usage. Analytical-grade reagents, H_2SO_4 and ethanol (Tianjin Kewei Reagent Co.) were used without any pretreatment. All solutions were prepared from de-ionized water (18 MΩ cm). Stainless-steel (SS) electrodes (316) were used as working electrode (WE) for PANI deposition. The deposited area was 0.283 cm^2 (6.0 mm in diameter) with other area insulated by a PTFE coating.

2.2. Preparation of PANI/SS electrodes

All electro-polymerization were carried out in a classic one-compartment cell using three-electrode configuration. Pt wire and saturated calomel electrode (SCE) were used as the counter electrode (CE) and reference electrode (RE), respectively. SS was polished to a mirror surface successively with emery paper (800#, 1200#, 2000#), rinsed with de-ionized water and immersed in ethanol ultrasonically for 5 min, then immersed in ionized water ultrasonically for 5 min.

PANI was electrodeposited on SS potentiostatically at 0.80 V from 1.0 M H_2SO_4 dissolving 0.10 M aniline monomer. Different polymerization times were applied in order to obtained PANI films with different thickness. Before electro-deposition, the electrolyte was degassed with pure nitrogen at least 20 min. PANI modified SS electrode (PANI/SS) was immersed in 1.0 M monomer-free H_2SO_4 for 48 h statically in order to expel aniline monomer and oligomer-PANI from the polymeric film. And the monomer-free H_2SO_4 was refreshed every 12 h and degassed with purified nitrogen before use.

2.3. Characterization of PANI/SS electrodes

The morphology of PANI was characterized by scanning electron microscopy (SEM, JEOL JSM-6700 F) and transmission electron microscopy (TEM, TECNAL G2 F20). The electrochemical performance of PANI/SS was characterized by CV, EIS, and charge/discharge methods. For CV and EIS methods, the configuration of the electrochemical cell was in three-electrode system. For the charge/discharge measurement, the configuration was in two-electrode system with identical PANI/SS electrodes applied as WE and CE.

All the polymerization experiments and EIS measurements were performed on PAR 273A (USA) controlled by a computer. CV testing was carried out on LK2005 (Lanlike Co. Ltd., Tianjin) controlled by a computer. The galvanostatic charge/discharge measurement was carried out on LAND CT2001A (Jinnuo Electronic Co. Ltd., Wuhan). The electrolytes used in the characterization of PANI/SS were degassed with purified nitrogen gas at least 20 min before use.

3. Theoretical calculation

3.1. Electrochemical measurements of PANI/SS

The supercapacitor performance of PANI/SS is characterized by CV, EIS, and galvanostatic charge/discharge method. The value for mass specific capacitance (C_s, F g^{-1}) can be calculated from the charge capability measured by CV and galvanostatic charge/discharge method, or obtained from the analysis of EIS data by equivalent circuit modeling.

3.1.1. Cyclic voltammetry

For CV method, the overall capacitance (C, F) is obtained from:

$$C = \frac{\mathrm{d}q}{\mathrm{d}E} = \frac{\mathrm{d}q}{\mathrm{d}t}\frac{\mathrm{d}t}{\mathrm{d}E} = i\frac{\mathrm{d}t}{\mathrm{d}E} = \frac{i}{\mathrm{d}E/\mathrm{d}t} = i/v \quad (1)$$

Here, i (A) is the *instantaneous* current in cyclic voltammograms, dE/dt (V s^{-1}) is the scanning rate (v, V s^{-1}). C (F) can be given by the average current ($\bar{i}$) divided by the scanning rate as [21]:

$$C = \frac{\bar{i}}{v} = \frac{1/(E_2 - E_1)\int_{E_1}^{E_2} i(E)\mathrm{d}E}{v} \quad (2)$$

Here, E_1, E_2 are the switching potentials in cyclic voltammetry. $\int_{E_1}^{E_2} i(E)\mathrm{d}E$ is voltammetric charge (q^*) obtained by integration of positive or negative sweep in cyclic voltammograms [28–30]. The upper-limit potential $E_2 = E_1 + vt$ (t is the time period of single positive or negative sweep), therefore, $\int_{E_1}^{E_2} i(E)\mathrm{d}E$ is transformed to $v\int_0^t i(t)\mathrm{d}t$ and Eq. (2) becomes:

$$C = \frac{\int_0^t i(t)\mathrm{d}t}{E_2 - E_1} \quad (3)$$

The C_s is calculated from $C_s = C/m$, here m (g) is the mass of PANI deposited on the substrate.

3.1.2. EIS measurement

The usefulness of EIS lies in the ability to distinguish contribution of the individual components of the investigated electrochemical system. Data recorded by EIS is modeling into an equivalent electrical circuit which consists of circuit elements such as the solution resistance (R_{sol}), the electrochemical double-layer capacitor produced from the charge separation at PANI/electrolyte interface (C_{dl}), and the bulk faradic impedance of PANI film. The bulk faradic impedance can be divided into pseudocapacitance (C_p) in parallel with a resistance which is the charge transfer resistance (R_{ct}) in redox process.

3.1.3. Galvanostatic charge/discharge

In charge/discharge experiment, the electrochemical cell is assembled in two-electrode system with PANI/SS electrode applied as both WE and CE. The PANI supercapacitor is charged to a desired voltage and then discharged at a constant current (i = const.) until the cell voltage between WE and CE decreases to 0.000 V. The average value for C_s can be deduced from the discharge curve according to:

$$C_s = \frac{i}{|(\mathrm{d}E/\mathrm{d}t) \times m|} \quad (4)$$

Here, m (g) is the total mass of PANI on the substrate as mentioned above; dE/dt (V s^{-1}) is the slope of the discharge curve. Because the curve can be treated as a linear one approximately, dE/dt is close to its mean value ($\Delta E/\Delta t$) where Δt (s) is the time period for the

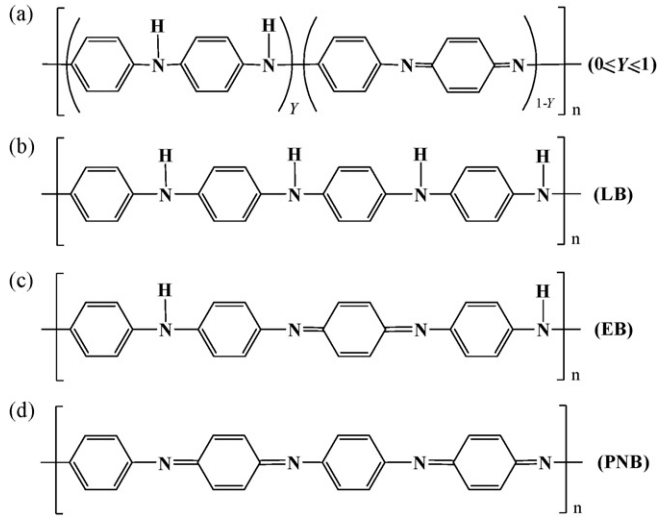

Scheme 1. Oxidation states of PANI.

overall potential decrease (ΔE, V) in discharge curve. Then Eq. (4) is transformed to:

$$C_s = \frac{i \times \Delta t}{\Delta E \times m} = \frac{Q}{\Delta E \times m} \quad (5)$$

Q (C) is the overall charge released during the discharge period.

Notice that in two-electrode system, the overall capacitance of the capacitor (C, F) is determined by the series equivalent circuit consisting of anode capacitance (C_a, F) and cathode capacitance (C_c, F) according to the equation:

$$\frac{1}{C_s} = \frac{1}{C_a} + \frac{1}{C_c} \quad (6)$$

If the two electrodes are exactly the same (i.e. $C_a = C_c$), Eq. (6) becomes:

$$C_s = \frac{1}{1/C_a + 1/C_c} = \frac{1}{2/C_a} = \frac{C_a}{2} \quad (7)$$

The C_s of the assembled PANI supercapacitor is just half the value of a single PANI/SS electrode.

Compared Eq. (3) applied for CV method and Eq. (5) applied for charge/discharge, the capacitance of PANI/SS is supposed to be determined by the potential window where PANI redox takes place and the corresponding charges stored in PANI.

3.2. Oxidation states and protonation of PANI

The generally accepted structure of PANI is described as Scheme 1a [31–33], where Y ($0 \le Y \le 1$) corresponds to the ratio of reduced unit and $1 - Y$ corresponds to the ratio of oxidized unit in PANI. The three separate oxidation states of PANI are: fully reduced form ($Y = 1$) which is designated as leucoemeraldine base (LB, Scheme 1b); half-oxidized form ($Y = 0.5$) which is designated as emeraldine base (EB, Scheme 1c); and fully oxidized form ($Y = 0$) designated as pernigraniline base (PNB, Scheme 1d).

All the three base forms LB, EB, and PNB can be protonated to corresponding salt forms designated as LH, ES and PNS (the anions in the structures are denoted as A^-), respectively. Duke and co-workers have investigated that the apparent pK_a values for LB and EB are −0.3 and 3 [34], which indicates that 50% of the nitrogen atoms for LB and EB will be protonated in the acidic medium where the pH is −0.3 and 3, respectively. As for the PANI-PNB form, because of the instability of protonated PANI-PNB [35–37], it is hard to investigate the apparent pK_a value for PNB. But the protonation of PNB will take place at pH 2 [38,39].

The redox of PANI has been investigated previously as shown in Scheme 2 [40,41]. When PANI-LB is oxidized to PANI-PNS form accompanied by doping of counter-anions in the electrolyte, one electron of each nitrogen atom is lost, accompanied by one counter-anion doped into PANI. And the charge capability for each repeated unit in PANI reaches the maximum value. The redox potentials of a single PANI fiber in 1.0 M H_2SO_4 have been investigated by Brett and co-workers [42]. The results showed that the oxidation of PANI-LB to PANI-ES takes place at $E_1 = 0.15$ V and PANI-ES to PANI-PNS takes place at $E_2 = 0.76$ V.

3.3. Estimation of maximum value

In order to estimate the theoretical value, several assumptions are made as following:

(1) The PANI nanofiber is solid and the entire surface is applied in charge storage producing the electric double-layer capacitance.
(2) The protonated PANI-PNS form is stable in 1.0 M H_2SO_4.
(3) The diffusion process of counter-anions (HSO_4^-) is fast enough and has no effect on the faradic reaction of PANI.
(4) The PANI film has high conductivity under various conditions.

Firstly, based on Assumption 1, the maximum value for electrical double-layer capacitance of PANI can be estimated as the value for a single-wall carbon nanotube in 1.0 M H_2SO_4 (in fact, it is much lower than that of the single-wall carbon nanotube because of its low specific surface area). The maximal value for single-wall carbon nanotubes, with diameter of 30 nm, is 320 F g^{-1} in Ref. [7]. Based on Assumptions 2 and 3, 100% of the PANI will be involved in charge storage with one counter-anion A^- doped to every nitrogen atom during the redox (as shown in Scheme 3). Finally, based on Assumptions 3 and 4, the redox process takes place in the PANI film is the same as that takes place in a single PANI fiber. The redox potential for PANI-LB/PANI-ES and PANI-ES/PANI-PNB is 0.15 and 0.76 V, respectively [42]. And all numbers in the calculation has 2 significant figures.

As shown in Scheme 3, the charge stored in PANI produced from faradic reaction (Q_p, C) is:

$$Q_p = 1nF \quad (8)$$

Here, n (mole) is the number of moles of aniline repeated units in PANI, F is the Faraday constant, 9.64853×10^4 C mol^{-1}. The pseudocapacitance (C_p, F) can be calculated from Q_p as:

$$C_p = \frac{Q_p}{\Delta E} \quad (9)$$

Here, ΔE is the potential window for LB oxidized to PNS. Then, the specific pseudocapacitance (C_{ps}, F g^{-1}) of PANI is:

$$C_{ps} = \frac{C_p}{m} = \frac{Q_p}{\Delta E \times m} \quad (10)$$

Here, m changes successively during electrochemical experiment due to the doping/dedoping of anions. Therefore, the mass of unprotonated PANI-LB form is used as the basis for estimating the maximum specific capacitance.

As for PANI with 1 mole of aniline repeat units, the faradic charge storage Q_p is:

$$Q_p = 1 \times 1 \times 9.64853 \times 10^4 = 96485.3\ \text{C} \quad (11)$$

The potential window is $\Delta E = E_2 - E_1 = 0.76\ \text{V} - 0.15\ \text{V} = 0.61$ V. The mass of PANI-LB with 1 mole of repeat aniline units is 91.1 g. Therefore, the C_{ps} is:

$$C_{ps} = \frac{Q_p}{\Delta E \times m} = \frac{96485.3}{0.61 \times 91.1} = 1736\ \text{F g}^{-1} = 1.7 \times 10^3\ \text{F g}^{-1} \quad (12)$$

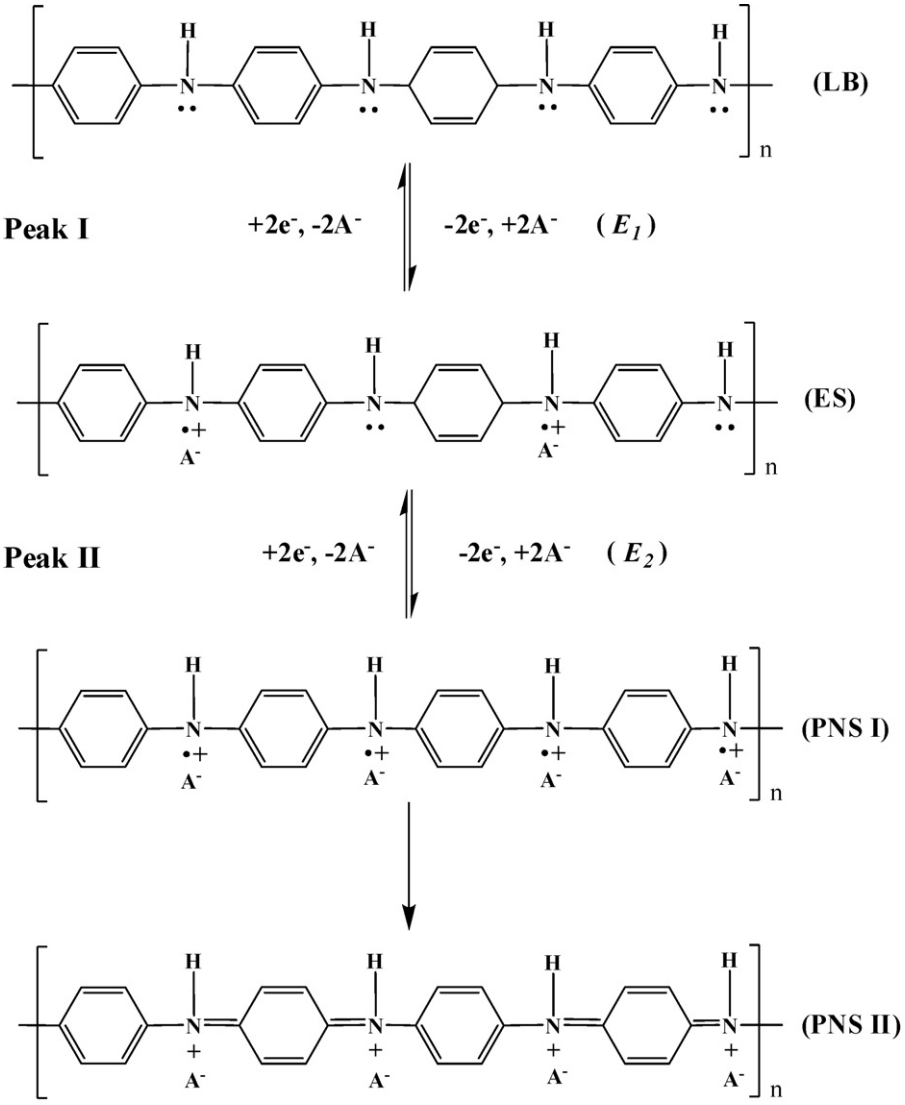

Scheme 2. Redox reaction of PANI in 1.0 M H_2SO_4.

As for electrical double-layer capacitance, the maximum value is regarded as 320 F g^{-1} as discussed above. The theoretical specific capacitance of PANI, which is a combination of pseudocapacitance with electrical double-layer capacitance, is 2.0×10^3 F g^{-1}. This value is the theoretical C_s for a single PANI electrode. And for the two-electrode system where two identical PANI/SS electrodes are applied as WE and CE, the overall C_s of the assembled PANI supercapacitor is:

$$C_s = \frac{1}{2} \times 2.0 \times 10^3 = 1.0 \times 10^3 \text{ F g}^{-1} \quad (13)$$

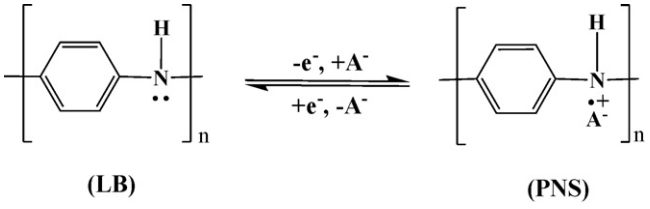

Scheme 3. Redox between PANI-LB and PANI-PNS.

4. Experimental results and discussion

4.1. Morphology of PANI

The morphology of PANI deposited on SS substrate was characterized by both SEM and TEM (Fig. 1). The SEM image indicates that the PANI is in nanofibrillar morphology under our experimental condition. Additionally, the TEM image (inserted on top-right corner of Fig. 1) indicates that the PANI nanofiber has a coarse surface and is in heterogeneous form. The nanofiber just like an aggregation of nanoparticles which have dense parts covered with loose materials. The coarse surface has positive effect on the specific surface area of PANI nanofibers and the diffusion of counter-anions, but the heterogeneous form has negative effect on the conductivity of PANI. All these factors should be considered in designing of PANI supercapacitor with large specific capacitance.

4.2. Cyclic voltammetry

PANI/SS electrode with a deposited charge (Q_{dep}) of 2.09 C cm^{-2} was cycled in the potential ranging from 0.000 to 0.800 V at various

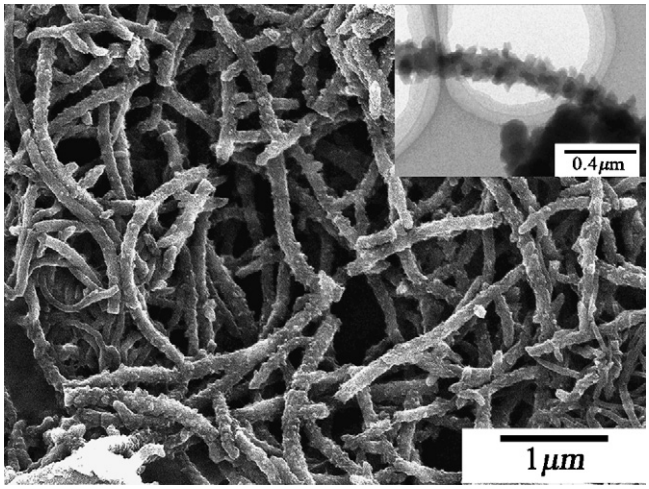

Fig. 1. SEM images of PANI on the substrate (TEM image inset at top-right corner).

scanning rates. The corresponding cyclic voltammograms are presented in Fig. 2a. Peaks AA′ correspond to the first redox process (LB/ES, Scheme 2), Peaks BB′ are supposed to represent the by-products and intermediates of hydroquinone/benzoquinone redox [43–45] and Peaks CC′ correspond to the second redox process (ES/PNS, Scheme 2). The relationship between the peak current density (j_p) and the square root of scanning rates ($v^{1/2}$) as well as that between the peak potential (E_p) and $v^{1/2}$, are collinear for both Peak A′ and Peak C (Fig. 2b). These results demonstrate that the diffusion process is the rate determining step during the redox of

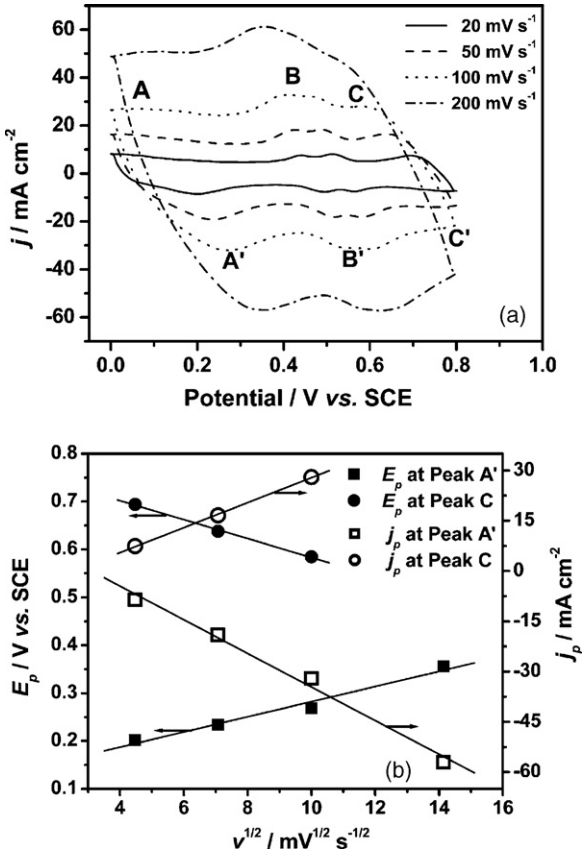

Fig. 2. (a) Cyclic voltammograms of PANI/SS and (b) the relationship between peak potentials and peak current densities *vs.* square root of scanning rates, $v^{1/2}$ from Fig. 2a.

Table 1
The C_s of PANI/SS electrodes at different scanning rates.

Scanning rate (mV s^{-1})	Area specific capacitance (mF cm^{-2})	Mass specific capacitance (F g^{-1})
20	281	418
50	262	391
100	230	342
200	196	292

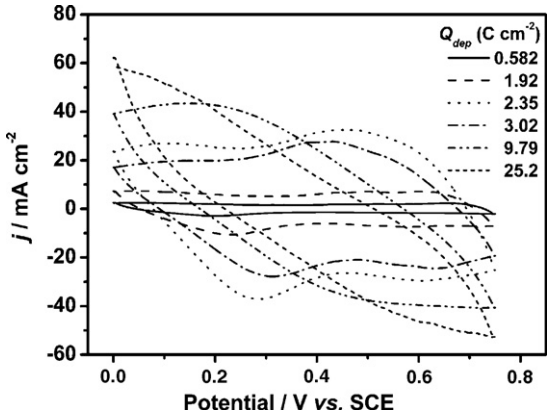

Fig. 3. Cyclic voltammograms of PANI/SS with different Q_{dep}.

PANI. Therefore the percentage of PANI effective for capacitance, which is influenced by the diffusion of counter-anions, is less than 100%. The C_s (capacitance per unit mass of material, F g^{-1}) and area specific capacitance (capacitance per unit deposited area, mF cm^{-2}) under different scanning rates are listed in Table 1. The results indicate that by increasing the scanning rate from 20 to 200 mV s^{-1}, the specific capacitance of PANI supercapacitor decreases.

Fig. 3 presents the cyclic voltammograms of PANI/SS with Q_{dep} increasing from 0.582 to 25.2 C cm^{-2}. The current peaks in Fig. 3 are distorted into a broader one with a larger Q_{dep}. Finally, they disappear when Q_{dep} reaches 9.79 C cm^{-2}. The increase in peak width at the half height implies a decrease in the electron transfer rate in PANI film [46]. Because the thickness of PANI film is in proportion to the Q_{dep}, it also confirms a slower electron transfer in a thicker PANI film. The relationship between the specific capacitance and Q_{dep} is shown in Fig. 4. When Q_{dep} increases from 0.582 to 2.35 C cm^{-2}, specific capacitance increase and reach the maxima with Q_{dep} equal to 2.35 C cm^{-2}, and the highest values in Fig. 4 are 920 mF cm^{-2} and 608 F g^{-1}, respectively. Further increasing Q_{dep} to 25.2 C cm^{-2}, the specific capacitance decreased gradually.

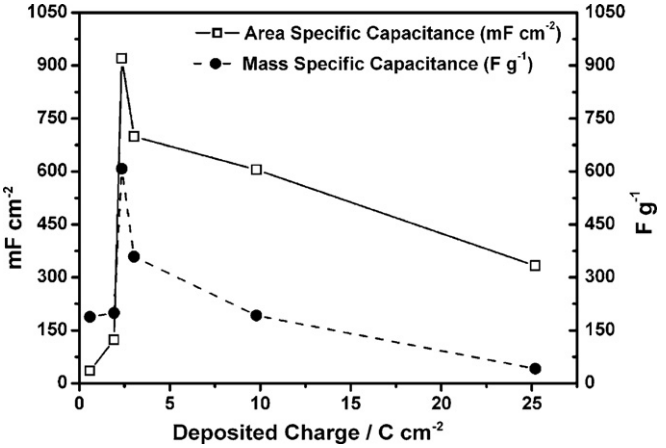

Fig. 4. Relationship between specific capacitances and Q_{dep} of the PANI/SS in Fig. 3.

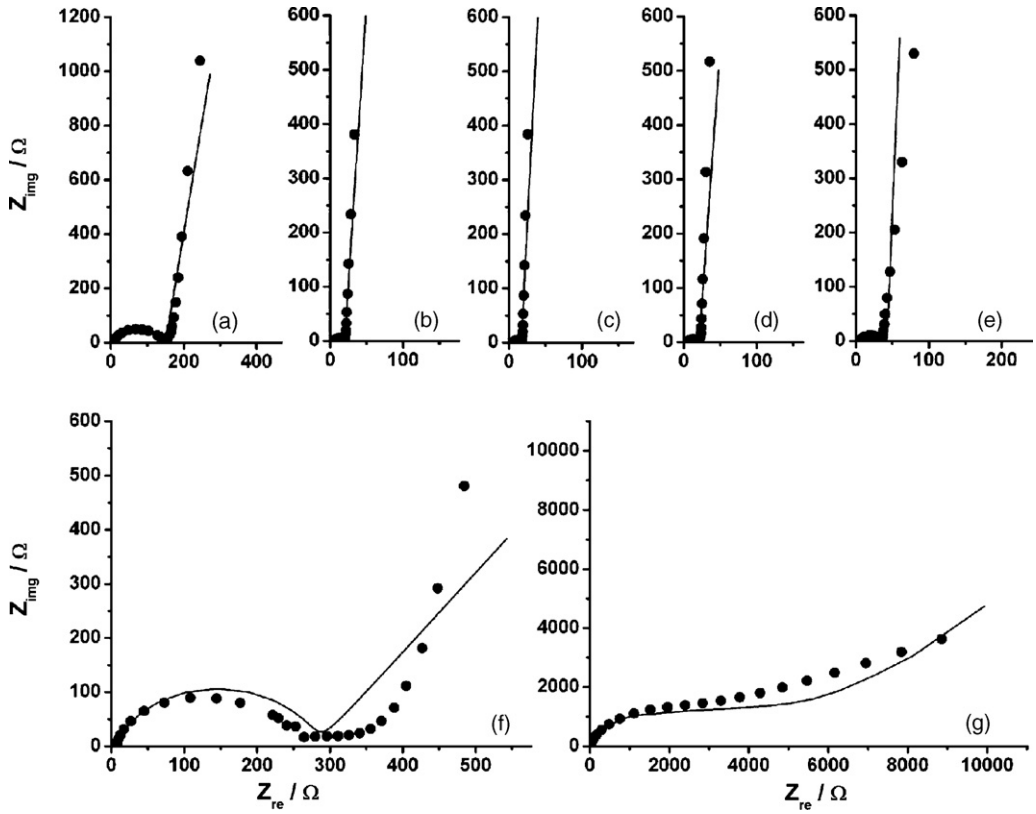

Fig. 5. Nyquist plots of PANI/SS at potential of (a) 0.000, (b) 0.200, (c) 0.400, (d) 0.550, (e) 0.600, (f) 0.750, and (g) 0.800 V in 1.0 M H_2SO_4. Dots denote the experimental values while the line represents the fitting of the data to the equivalent circuit in Fig. 6 using the parameters in Table 2.

4.3. EIS measurement

The conductivity of PANI depends on both the oxidation state and the doping degree of PANI. During charge/discharge, the potential of PANI/SS electrode changes successively resulting from the corresponding change in oxidation state of PANI. The capacitance and conductivity of PANI at different oxidation state were studied by EIS technique under various potentials. The impedance spectra are shown as Nyquist plots in Fig. 5a–g. All the plots consist of a distorted semicircle in the high frequency (HF) region and a straight line in the low frequency (LF) region. The HF intercept with the real axis is equal to the solution resistance (R_{sol}) and the diameter of the semicircle is equal to the electrode resistance which arises from the charge transfer resistance (R_{ct}) in PANI film. As well known, a vertical line is equal to an equivalent circuit consisting of a resistance in parallel with an ideal capacitor. However, the inclination from the vertical in the very low frequency range is often observed for the experimental result which is attributed to a non-homogeneity film [47,48]. Therefore, constant phase elements (CPE) are applied in the equivalent circuit for the simulation of the impedance data. CPE is defined by:

$$Z_{\mathrm{CPE}} = T_{\mathrm{CPE}}(j\omega)^{-n}_{\mathrm{CPE}}$$

where T and n are frequency-independent constants and ω is the angular frequency. The exponent n is a correction factor related to the roughness of electrode surfaces. The values for n are ranging between 0 and 1. $n = 1$ denotes the CPE element is an ideal capacitor, while $n = 0$ and 0.5, denotes a resistance and Warburg behavior, respectively.

The proper equivalent circuit to simulate the impedance data of PANI/SS is shown in Fig. 6 [49]. CPE_1 and CPE_2 are expressed as a capacity at non-homogeneous electrode surfaces and ionic diffusion process in the polymeric film, respectively [50]. Table 2 lists the fitting values for the elements in Fig. 6 obtained by the simulation of impedance spectra in Fig. 5. The mean error of modulus is less than 0.7% indicating that these fitting values are highly trustful. n_1 values changes in a narrow range which may be caused by the shrink-swell behavior of PANI upon the electrochemical oxidation and reduction accompanied by dop-

Table 2
Fitting values for the equivalent circuit elements in Fig. 6 by the simulation of impedance spectra in Fig. 5.

Element	Potential (V)						
	0.000	0.200	0.400	0.550	0.600	0.750	0.850
R_{sol} (Ω)	6.318	5.034	4.24	4.472	5.104	5.855	6.629
CPE_1 (μF)	12.58	14.12	25.81	20.77	11.75	53.08	33.63
n_1	0.7867	0.7497	0.6835	0.7053	0.7597	0.8295	0.878
R_{ct} (Ω)	145.3	15.00	13.06	16.60	31.10	277.3	1158
CPE_2 (Fg^{-1})	212.4	365.0	363.2	445.0	411.0	323.5	11.70
n_2	0.9227	0.9701	0.9784	0.9673	0.9482	0.6200	0.2738
Mean error	3.685E−03	1.490E−03	1.202E−03	1.552E−03	3.533E−03	6.185E−03	6.730E−03

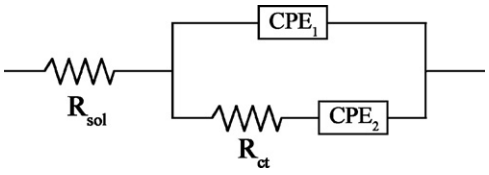

Fig. 6. Equivalent circuit for the simulation of the EIS spectra of PANI/SS.

ing/dedoping of counter-anions. n_2 values denote the capacitive nature of the system. The value of n_2 at ~0.9 indicates the highly capacitive nature. At 0.750 V, the value of $n_2 = 0.62$ implies the performance of PANI/SS deviates gradually from a capacitor to Warburg behavior. And at 0.850 V (PANI at fully oxidized state), $n_2 = 0.2738$ indicates the resistive nature of PANI/SS electrode. The charge transfer resistance (R_{ct}) increases in the order as $R_{ct,\,0.400\,V} < R_{ct,\,0.200\,V} < R_{ct,\,0.550\,V} < R_{ct,\,0.600\,V} < R_{ct,\,0.000\,V} < R_{ct,\,0.750\,V} < R_{ct,\,0.850\,V}$. This phenomenon is consistent with the fact that the PANI-ES form (exists at 0.400 V) is the most conductive form. And the redox state of PANI at 0.000, 0.750, and 0.850 V corresponding to the fully reduced or oxidized form are poor for charge transfer. CPE_1 is related to the double-layer capacitance producing on the surface of PANI nanofiber while CPE_2 is related to the pseudocapacitance. The value of CPE_1 is much less than that of CPE_2, so the specific capacitance of PANI/SS is regarded to be the value of CPE_2 approximately. The C_s is found out to range from 11.7 to 445.0 F g^{-1} and reaches the maximum at the potential of 0.550 V. The result indicates that both the conductivity of PANI and the cell potential affects the degree of PANI redox which determines the capacitance.

Then, PANI/SS electrodes with different Q_{dep} were also studied. The corresponding impedance spectra are shown as Nyquist plots in Fig. 7a–e. The values for the equivalent circuit elements in Fig. 6 obtained by the simulation of the impedance spectra in Fig. 7 are listed in Table 3. The value for R_{ct} increases by increasing the Q_{dep} which indicates that a slower electron transfer in a thicker PANI film. This phenomenon is consistent with that observed by CV method in Section 4.2. However, there is no obvious relationship between C_s of PANI/SS and Q_{dep} in the range from 0.337 to 0.929 C cm^{-2}. The maximum is 365.5 F g^{-1} with Q_{dep} equal to 0.701 C cm^{-2}.

4.4. Galvanostatic charge/discharge

Galvanostatic charge/discharge method was also applied to characterize the PANI/SS in 1.0 M H_2SO_4. The electrochemical cell for this method was configured in two-electrode system where two identical PANI/SS electrodes were applied as the WE and CE, respectively. Fig. 8 represents the typical charge/discharge curves over a potential window from 0.000 V to 0.600, 0.750, and 0.800 V at 0.10, 0.20, 0.40, and 0.80 mA, respectively. As shown in Fig. 8a, the cathodic discharge process shows the mirror image of their corresponding anodic charge counterparts on both curves which indicates that the PANI/SS system exhibits an ideally capacitive behavior in the potential window ranging from 0.000 to 0.600 V.

Table 3
Fitting values for the equivalent circuit elements in Fig. 6 by the simulation of impedance spectra in Fig. 7.

Element	Deposited charge (Q_{dep}) (C cm^{-2})				
	0.337	0.701	0.712	0.727	0.929
R_{sol} (Ω)	8.337	9.151	11.47	8.906	11.96
CPE_1 (μF)	20.81	9.988	8.052	31.13	5.533
n_1	0.6369	0.7211	0.7873	0.6565	0.8006
R_{ct} (Ω)	14.30	31.16	47.48	72.81	88.33
CPE_2 (F g^{-1})	269.5	365.6	256.5	267.1	315.3
n_2	0.9555	0.9766	0.9806	0.9764	0.9784
Mean error	7.348E−03	9.793E−04	1.936E−03	1.870E−03	1.845E−03

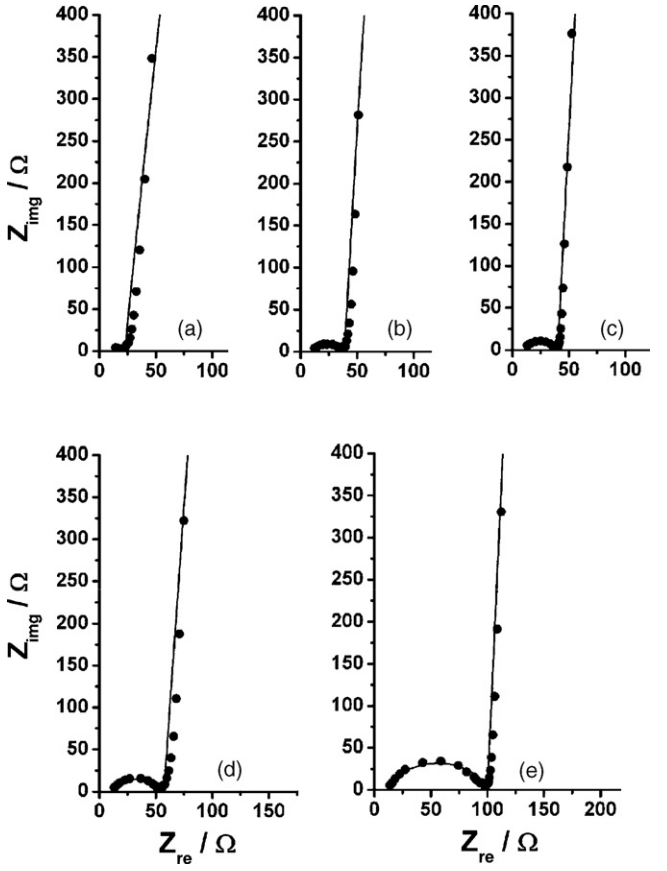

Fig. 7. Nyquist plots of PANI/SS electrodes with Q_{dep} equal to (a) 0.337, (b) 0.701, (c) 0.712, (d) 0.727, and (e) 0.929 C cm^{-2} in 1.0 M H_2SO_4. Dots denote experimental values while the line represents the fitting of the data to the equivalent circuit in Fig. 6 using the parameters in Table 3.

Extending the upper-limit to 0.750 and 0.800 V (Fig. 8b and c), the IR drops become significant resulting in an asymmetry in charge/discharge curves. The IR drop is attributed to the equivalent series resistance (ESR) of PANI/SS system which arises from the resistance of both the electrolyte and the PANI film. When higher potentials applied, the PANI/SS system is more like a resistance rather than a capacitor. The increase in the resistance of the PANI film causes the increase in IR drop. On the other hand, under the same potential, the increase in IR drop with increasing the constant current is mainly attributed to the resistance of the electrolyte.

The C_s values of PANI/SS system in Fig. 8 are listed in Table 4. Being carried out in two-electrode system, the C_s value of one

Table 4
The C_s values of PANI/SS in Fig. 8.

Potential (V)	Current (mA)	C_s (F g^{-1})	
		Two-electrode system	One single PANI/SS
0.600	0.10	242.5	494.4
	0.20	248.5	497.0
	0.40	243.3	486.7
	0.80	236.5	473.0
0.750	0.10	252.6	505.2
	0.20	242.6	485.3
	0.40	227.6	455.1
	0.80	208.4	416.8
0.800	0.10	230.1	460.1
	0.20	223.0	446.0
	0.40	208.2	416.4
	0.80	185.1	370.1

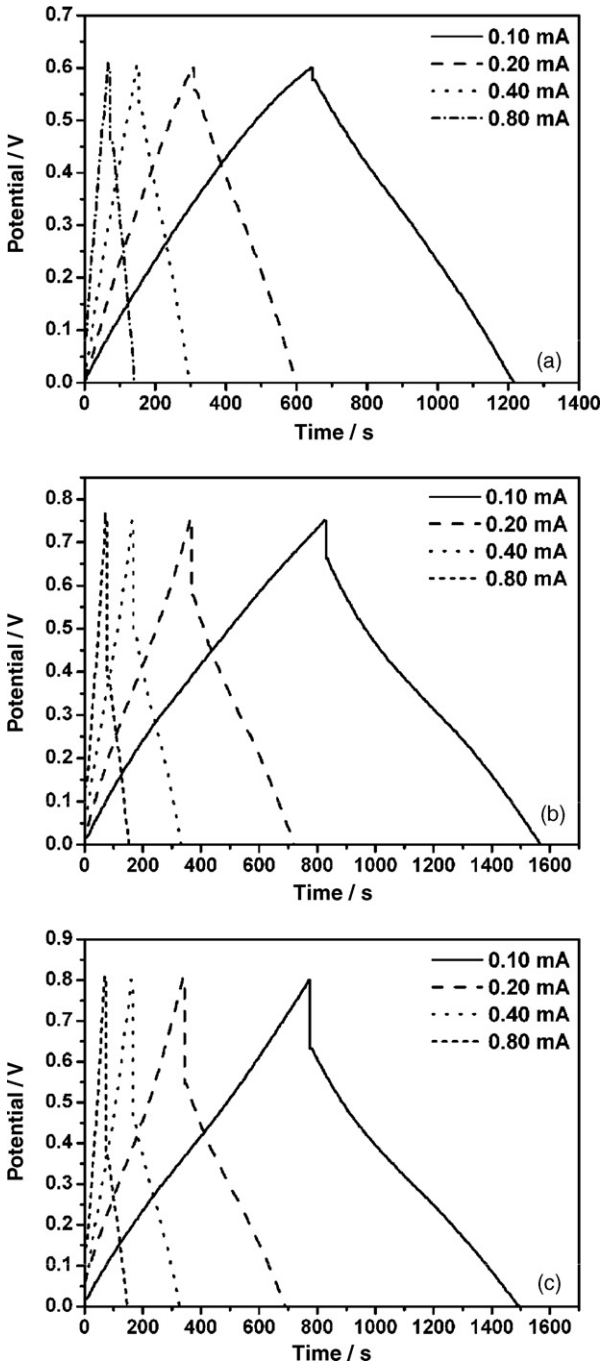

Fig. 8. Galvanostatic charge/discharge curves of PANI/SS electrode.

single PANI/SS electrode in the galvanostatic charge/discharge measurement is twice as large as the overall C_s value. For a certain upper-limit potential, the C_s increases with decreasing the charge/discharge current. This is attributed from the more counter-anions diffusing into/out PANI during the charge/discharge process at the lower charge/discharge current. This phenomenon is similar to that observed in CV experiments. On the other hand, for a certain current, the C_s decreases with increasing the upper-limit potential. As mentioned above, under higher potential is, the PANI/SS system is more like a resistance rather than a capacitor. The results for upper-limit potential at 0.600 V appeared in the table, which is highly reproductive, also indicate that the C_s with charge/discharge current at 0.10 mA is less than that at 0.20 mA, even less than 0.10 mA at 0.750 V.

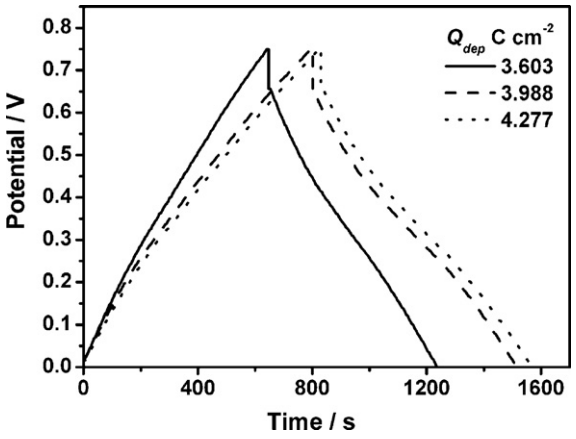

Fig. 9. Galvanostatic charge/discharge curves of PANI/SS electrodes with different Q_{dep}.

The reason responsible for this phenomenon is unclear so far.

The performance of PANI/SS electrodes with different Q_{dep} was also studied in the potential window from 0.000 to 0.750 V. Fig. 9 shows the charge/discharge curves at the constant current of 0.10 mA. The C_s value of PANI/SS with different Q_{dep} tested at 0.10 mA as well as at 0.20, 0.40, and 0.80 mA are listed in Table 5. For a certain Q_{dep}, the PANI/SS supercapacitor has a lower capacitance at a higher current which is consistent with the results above. The maximum C_s is obtained from the PANI/SS with Q_{dep} at 3.998 C cm^{-2} discharge at 0.10 mA.

4.5. Comparison between experimental value and theoretical one

From the results above, the maximum C_s obtained from CV, EIS, and galvanostatic charge/discharge methods in present work is 608, 445.0, and 524.9 F g^{-1}, respectively, which is only 30%, 22%, and 26% of the theoretical one. As for EIS method, the C_s value is approximately regarded as the pseudocapacitance during the calculation in Section 4.3 resulting in a smaller value than that of the other two methods. During CV measurement, the potential of WE is controlled relative to RE. Therefore, PANI on WE will undergo redox in the potential window which is controlled exactly. However, during charge/discharge measurement, the controlled parameter is the potential difference between WE and CE. Even if the experimental parameter (potential window) of charge/discharge measurement is the same as that of CV, both the electrodes would undergo redox in a narrower potential window compared to that in CV. As a result, the charge storage measured by galvanostatic charge/discharge method is less than that obtained by CV.

The difference between the theoretical value and the experimental one shows that the effective part of pure PANI contributing to capacitance is low. This is attributed from the fact that the diffusion of dopants (counter-anions) is the rate determining step during the redox of PANI. Either decreasing the scanning rate of CV or the current of galvanostatic charge/discharge will increase

Table 5
The C_s values of PANI/SS in Fig. 9.

Deposited charge (Q_{dep}) (C cm^{-2})	C_s (one single PANI/SS electrode) (F g^{-1})			
	Charge/discharge current (mA)			
	0.10	0.20	0.40	0.80
3.603	480.0	439.3	400.3	351.4
3.988	524.9	474.9	429.3	376.4
4.277	505.2	485.3	455.1	416.7

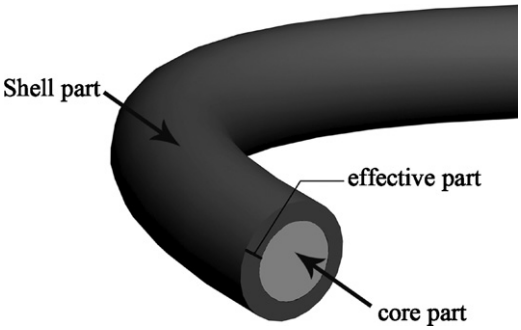

Fig. 10. Core-shell model of PANI utilized in charge storage influenced by diffusion of dopants.

an amount of dopants into/out the PANI, and thus results in the increase of capacitance of PANI. The influence of diffusion process on the PANI capacitance is given in Fig. 10. The dark shell stands for the part where the insertion/expulsion of counter-anions can take place, and the grey core stands for the conductive part of PANI nanofiber where no change occurs during the charge/discharge process. Therefore, the grey core has no contribution to the capacitance and only the dark shell is available for capacitance. The ratio of the dark shell to the whole PANI nanofiber represents the proportion of PANI generating capacitance.

The PANI nanofiber must be conductive for electron transfer during the redox reaction of PANI. As mentioned in Section 4.1, the PANI nanofiber has actually a heterogeneous structure in present work. The protonated polyaniline in 1.0 M H_2SO_4 was found to behave as archipelago of metallic "islands" (the crystalline structure) separated from one another by insulated "beaches" (the amorphous structure) [51–56]. Therefore, the structure of PANI nanofiber is like conductive islands dispersed in an insulated sea. The model in Fig. 10 only represents the conductive islands in PANI nanofibers. However, the insulated part which has no contribution to the capacitance occupies a considerable proportion of the PANI nanofiber. Based on these factors, the experimental results obtained by CV, EIS, and galvanostatic charge/discharge methods were found to be much less than the theoretical one.

5. Conclusion

The theoretical maximum specific capacitance (C_s) of PANI/SS supercapacitor is estimated to be $2.0 \times 10^3\,F\,g^{-1}$. Taking the diffusion of counter-anions and the conductivity of PANI into consideration, only a small part of PANI has contribution to capacitance. Practically, the maximum C_s value measured by CV, EIS, and galvanostatic charge/discharge methods in present work is 608, 445.0, and $524.9\,F\,g^{-1}$, respectively. Firstly, the diffusion of counter-anions in PANI is confirmed to be the rate determining step during the redox. This process degrades the charge/discharge capability of PANI. The porosity of PANI film is a benefit for sufficient contact between the counter-anions and the PANI. Secondly, the PANI nanofiber obtained in present work is a heterogeneous structure. The insulated part is not efficient for charge storage. Based on these factors, the experimental values are much less than the theoretical one. In order to improve the performance of supercapacitors, the homogeneous PANI nanofibers with large surface area (low diameter and coarse surface) should be applied to modify the substrate.

Acknowledgements

This work was supported by the Program of Introducing Talents of Discipline to Universities (No: B06006), Program for Innovative Research Team in University, the Program for New Century Excellent Talents in University and Lanlike (Tianjin) Chem-Electronic Hi-Tech Ltd.

References

[1] E. Faggioli, P. Rena, V. Danel, X. Andrieu, R. Mallant, H. Kahlen, J. Power Sources 84 (1999) 261–269.
[2] R.A. Huggins, Solid State Ionics 134 (2000) 179–195.
[3] A. Burke, J. Power Sources 91 (2000) 37–50.
[4] R. Kotz, M. Carlen, Electrochim. Acta 459 (2000) 2483–2498.
[5] E. Frackowiak, F. Beguin, Carbon 39 (2001) 937–950.
[6] B.E. Conway, W.G. Pell, J. Solid State Electron. 7 (2003) 637–644.
[7] M.J. Bleda-Martinez, J.A. Macia-Agullo, D. Lozano-Castello, E. Morallon, D. Cazorla-Amoros, A. Linares-Solano, Carbon 43 (2005) 2677–2684.
[8] I.H. Kim, J.H. Kim, Y.H. Lee, K.B. Kim, J. Electrochem. Soc. 152 (2005) A2170–A2178.
[9] M. Mastragostino, C. Arbizzani, F. Soavi, J. Power Sources 97–98 (2001) 812–815.
[10] M. Mastragostino, C. Arbizzani, F. Soavi, Solid State Ionics 148 (2002) 493–498.
[11] N.S. Sariciftci, M. Bartonek, H. Kuzmany, H. Neugebauer, A. Neckel, Synth. Met. 29 (1989) 193–202.
[12] H. Reiss, Synth. Met. 30 (1989) 257–263.
[13] W.C. Chen, T.C. Wen, J. Power Sources 117 (2003) 273–282.
[14] W.C. Chen, T.C. Wen, H.S. Teng, Electrochim. Acta 48 (2003) 641–649.
[15] T.C. Girija, M.V. Sangaranarayanan, J. Power Sources 156 (2006) 705–711.
[16] K.R. Prasad, N. Munichandraiah, J. Power Sources 112 (2002) 443–451.
[17] K.R. Prasad, N. Munichandraiah, J. Electrochem. Soc. 149 (2002) A1393–A1399.
[18] H.H. Zhou, H. Chen, S.L. Luo, G.W. Lu, W.Z. Wei, Y.F. Kuang, J. Solid State Electron. 9 (2005) 574–580.
[19] V. Gupta, N. Miura, Electrochem. Solid State Lett. 8 (2005) A630–A632.
[20] T.C. Girija, M.V. Sangaranarayanan, Synth. Met. 156 (2006) 244–250.
[21] R.Y. Song, J.H. Park, S.R. Sivakkumar, S.H. Kim, J.M. Ko, D.Y. Park, S.M. Jo, D.Y. Kim, J. Power Sources 166 (2007) 297–301.
[22] C.C. Hu, W.Y. Li, J.Y. Lin, J. Power Sources 137 (2004) 152–157.
[23] Y.K. Zhou, B.L. He, W.J. Zhou, J. Huang, X.H. Li, B. Wu, H.L. Li, Electrochim. Acta 49 (2004) 257–262.
[24] V. Gupta, N. Miura, Electrochim. Acta 52 (2006) 1721–1726.
[25] V. Gupta, N. Miura, J. Power Sources 157 (2006) 616–620.
[26] S.R. Sivakkumar, W.J. Kim, J.A. Choi, D.R. MacFarlane, M. Forsyth, D.W. Kim, J. Power Sources 171 (2007) 1062–1068.
[27] H. Mi, X. Zhang, X. Ye, S. Yang, J. Power Sources 176 (2008) 403–409.
[28] W.G. Pell, B.E. Conway, J. Electroanal. Chem. 500 (2001) 121–133.
[29] C.C. Hu, T.W. Tsou, Electrochem. Commun. 4 (2002) 105–109.
[30] J.K. Chang, C.H. Huang, W.T. Tsai, M.J. Deng, I.W. Sun, J. Power Sources 179 (2008) 435–440.
[31] H.T. Deng, G.J. Van Berkel, Anal. Chem. 71 (1999) 4284–4293.
[32] R. Madathil, S. Ponrathnam, H.J. Byrne, Polymer 45 (2004) 5465–5471.
[33] H.S. Kolla, S.P. Surwade, X. Zhang, A.G. MacDiarmid, S.K. Manohar, J. Am. Chem. Soc. 127 (2005) 16770–16771.
[34] D. Orata, D.A. Buttry, J. Am. Chem. Soc. 109 (1987) 3574–3581.
[35] G.E. Asturias, A.G. MacDiarmid, R.P. McCall, A.J. Epstein, Synth. Met. 29 (1989) 157–162.
[36] A.G. MacDiarmid, S.K. Manohar, J.G. Masters, Y. Sun, H. Weiss, A.J. Epstein, Synth. Met. 41 (1991) 621–626.
[37] N. Chandrakanthi, M.A. Careem, Polym. Bull. 45 (2000) 113–120.
[38] Z. Ping, G.E. Nauer, H. Neugebauer, J. Theiner, A. Neckel, J. Chem. Soc., Faraday Trans. 93 (1997) 121–129.
[39] E.N. Konyushenko, J. Stejskal, I. Sedenkova, M. Trchova, I. Sapurina, M. Cieslar, J. Prokes, Polym. Int. 55 (2006) 31–39.
[40] A. Watanabe, K. Mori, Y. Iwasaki, Y. Nakamura, S. Niizuma, Macromolecules 20 (1987) 1793–1796.
[41] H. Kuzmany, N.S. Sariciftci, H. Neugebauer, A. Neckel, Phys. Rev. Lett. 60 (1988) 212–215.
[42] R. Pauliukaite, C.M.A. Brett, A.P. Monkman, Electrochim. Acta 50 (2004) 159–167.
[43] T. Kobayashi, H. Yoneyama, H. Tamura, J. Electroanal. Chem. 177 (1984) 293–297.
[44] E.M. Genies, C. Tsintavis, J. Electroanal. Chem. 195 (1985) 109–128.
[45] A. Kitani, M. Kaya, J. Yano, K. Yoshikawa, K. Sasaki, Synth. Met. 18 (1987) 341–346.
[46] E.S. David, P. Su-Moon, J. Electrochem. Soc. 135 (1988) 2254–2262.
[47] N.G. Skinner, E.A.H. Hall, Synth. Met. 63 (1994) 133–145.
[48] C. Gabrielli, H. Takenouti, O. Haas, A. Tsukada, J. Electroanal. Chem. 302 (1991) 59–89.
[49] U. Retter, A. Widmann, K. Siegler, H. Kahlert, J. Electroanal. Chem. 546 (2003) 87–96.
[50] M.A. Vorotyntsev, J.P. Badiali, G. Inzelt, J. Electroanal. Chem. 472 (1999) 7–19.
[51] K. Mizoguchi, M. Nechtschein, J.P. Travers, C. Menardo, Phys. Rev. Lett. 63 (1989) 66–69.
[52] A. Ray, G.E. Asturias, D.L. Kershner, A.F. Richter, A.G. MacDiarmid, A.J. Epstein, Synth. Met. 29 (1989) 141–150.
[53] Z.H. Wang, Phys. Rev. B 45 (1992) 4190–4202.
[54] R. Pelster, G. Nimtz, Phys. Rev. B 49 (1994) 12718–12723.
[55] R. Farchioni, P. Vignolo, G. Grosso, Phys. Rev. B 60 (1999) 15705–15713.
[56] J.P. Travers, A. Wolter, P. Rannou, M. Nechtschein, B. Gilles, D. Djurado, Synth. Met. 101 (1999) 838–1838.